EVIDENCE FOR $Z^0 \to e^+e^-$ AT THE CERN $\bar{p}p$ COLLIDER

The UA2 Collaboration

P. BAGNAIA [b], M. BANNER [f], R. BATTISTON [1,2], Ph. BLOCH [f], F. BONAUDI [b], K. BORER [a], M. BORGHINI [b], J.-C. CHOLLET [d], A.G. CLARK [b], C. CONTA [e], P. DARRIULAT [b], L. Di LELLA [b], J. DINES-HANSEN [c], P.-A. DORSAZ [b], L. FAYARD [d], M. FRATERNALI [e], D. FROIDEVAUX [b], G. FUMAGALLI [e], J.-M. GAILLARD [d], O. GILDEMEISTER [b], V.G. GOGGI [e], H. GROTE [b], B. HAHN [a], H. HÄNNI [a], J.R. HANSEN [b], P. HANSEN [c], T. HIMEL [b], V. HUNGERBÜHLER [b], P. JENNI [b], O. KOFOED-HANSEN [c], E. LANÇON [f], M. LIVAN [b,e], S. LOUCATOS [f], B. MADSEN [c], P. MANI [a], B. MANSOULIÉ [f], G.C. MANTOVANI [1], L. MAPELLI [b,3], B. MERKEL [d], M. MERMIKIDES [b], R. MØLLERUD [c], B. NILSSON [c], C. ONIONS [b], G. PARROUR [b,d], F. PASTORE [e], H. PLOTHOW-BESCH [b], M. POLVEREL [f], J-P. REPELLIN [d], A. RIMOLDI [e], A. ROTHENBERG [b], A. ROUSSARIE [f], G. SAUVAGE [d], J. SCHACHER [a], J.L. SIEGRIST [b], H.M. STEINER [b,4], G. STIMPFL [b], F. STOCKER [a], J. TEIGER [f], V. VERCESI [e], A.R. WEIDBERG [b], H. ZACCONE [f], J.A. ZAKRZEWSKI [b,5] and W. ZELLER [a]

[a] *Laboratorium für Hochenergiephysik, Universität Bern, Sidlerstrasse 5, Bern, Switzerland*
[b] *CERN, 1211 Geneva 23, Switzerland*
[c] *Niels Bohr Institute, Blegdamsvej 17, Copenhagen, Denmark*
[d] *Laboratoire de l'Accélérateur Linéaire, Université de Paris-Sud, Orsay, France*
[e] *Dipartimento di Fisica Nucleare e Teorica, Università di Pavia and INFN, Sezione di Pavia, Via Bassi 6, Pavia, Italy*
[f] *Centre d'Etudes Nucléaires de Saclay, France*

Received 11 August 1983

From a search for electron pairs produced in $\bar{p}p$ collisions at $\sqrt{s} = 550$ GeV we report the observation of eight events which we interpret as resulting from the process $\bar{p} + p \to Z^0 +$ anything, followed by the decay $Z^0 \to e^+ + e^-$ or $Z^0 \to e^+ + e^- + \gamma$, where Z^0 is the neutral Intermediate Vector Boson postulated by the unified electroweak theory. We use four of these events to measure the Z^0 mass

$M_Z = 91.9 \pm 1.3 \pm 1.4$ (systematic) GeV/c^2.

1. Introduction. The primary goal of the experimental program at the CERN $\bar{p}p$ Collider has been to search for the massive Intermediate Vector Bosons (IVB), which are postulated to mediate the electroweak interaction [1].

The recent observation of single isolated electrons with high transverse momentum in events with missing transverse energy [2,3] is consistent with the process $\bar{p} + p \to W^\pm +$ anything, followed by the decay $W^\pm \to e^\pm + \nu(\bar{\nu})$, where W is the charged IVB.

We report here the observation in the UA2 detector of eight events which we interpret in terms of the reaction

$$\bar{p} + p \to Z^0 + \text{anything}, \quad Z^0 \to e^+ + e^- \text{ or } e^+ + e^- + \gamma, \qquad (1)$$

[1] Gruppo INFN del Dipartimento di Fisica dell'Università di Perugia, Italy.
[2] Also at Scuola Normale Superiore, Pisa, Italy.
[3] On leave from INFN, Pavia, Italy.
[4] On leave from Department of Physics, University of California, Berkeley, CA, USA.
[5] On leave from Institute of Physics, University of Warsaw, Poland.

0.031-9163/83/0000–0000/$ 03.00

where Z^0 is the neutral IVB. The observation of these events, which have been found in a data sample corresponding to a total integrated luminosity of 131 nb^{-1}, agrees with the SU(2) × U(1) model and with the recent results of the UA1 experiment [4].

2. The detector. The experimental apparatus [5] is shown in fig. 1. At the centre of the apparatus a system of cylindrical chambers (the vertex detector) measures charged particle trajectories in a region without magnetic field. The vertex detector consists of: (a) four multi-wire proportional chambers having cathode strips with pulse height read-out at ±45° to the wires; (b) two drift chambers with measurement of the charge division on a total of 12 wires per track. These chambers are used both to obtain tracking information and to evaluate the most likely ionisation I (in units of equivalent minimum ionising particles, mip) associated with each track. From the reconstructed charged particle tracks the position of the event vertex is determined with a precision of ±1 mm in all directions.

The vertex detector is surrounded by an electromagnetic and hadronic calorimeter [6] (the central calorimeter), which covers the polar angle interval $40° < \theta < 140°$ and the full azimuth. This calorimeter is segmented into 240 cells, each covering 15° in ϕ and 10° in θ and built in a tower structure pointing to the centre of the interaction region. The cells are segmented longitudinally into a 17 radiation lengths thick electromagnetic compartment (lead-scintillator) followed by two hadronic compartments (iron-scintillator) of ~2 absorption lengths each. The light from each compartment is channelled to two photomultipliers (PMs) by means of BBQ-doped light guides on opposite sides of the cell.

In the angular region covered by the central calorimeter a cylindrical tungsten converter, 1.5 radiation lengths thick, followed by a cylindrical proportional chamber, is located just after the vertex detector. This chamber, named C5 (see fig. 1), has cathode strips at ±45° to the wires. We measure the pulse height on the cathode strips and the charge division on the wires. This device localises electromagnetic showers initiated in the tungsten with a precision of 3 mm.

For the first 15 nb^{-1} of integrated luminosity, collected during the Autumn of 1982, the azimuthal coverage of the central calorimeter was only 300°. The

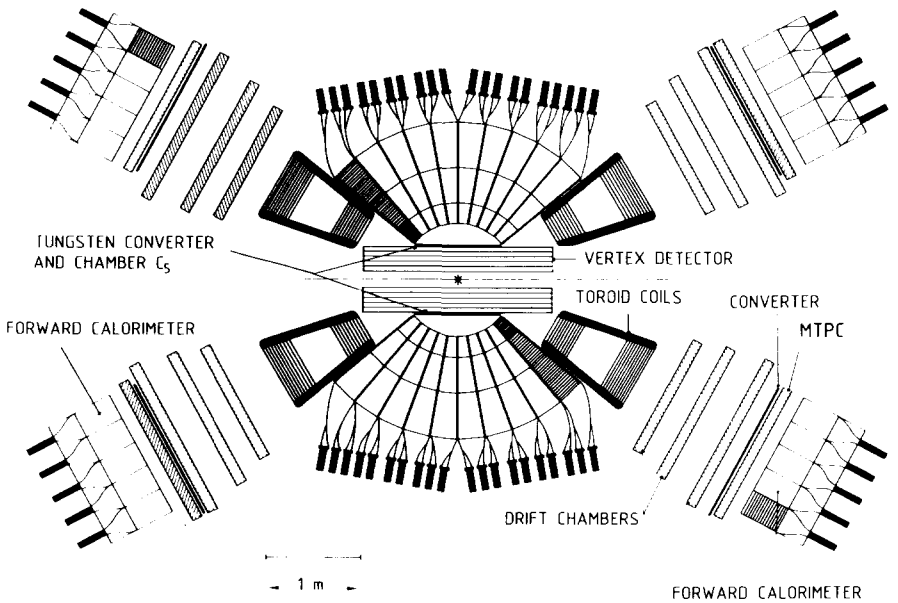

Fig. 1. Schematic detector assembly (cut in a plane containing the beam line).

remaining interval (±30° around the horizontal plane) was covered by a magnetic spectrometer which included a lead-glass wall, to measure charged and neutral particle production [7,8].

The two forward regions ($20° < \theta < 37.5°$ and $142.5° < \theta < 160°$), are each equipped with twelve toroidal magnet sectors with an average field integral of 0.38 Tm. Each sector is instrumented with:

(a) Three drift chambers [9] located after the magnetic field region. Each chamber consists of three planes, with wires at $-7°$, $0°$, $+7°$, with respect to the magnetic field direction.

(b) A 1.4 radiation lengths thick lead–iron converter, followed by a chamber [10] consisting of two pairs of layers of 20 diameter proportional tubes (MTPC), staggered by a tube radius and equipped with pulse height measurement. There is a 77° angle between the tubes of the two pairs of layers, with the tubes of the first one being parallel to the magnetic field direction. This device localises electromagnetic showers with a precision of $\lesssim 8$ mm.

(c) An electromagnetic calorimeter consisting of lead-scintillator counters assembled in ten independent cells, each covering 15° in ϕ and 3.5° in θ. Each cell is subdivided into two independent longitudinal sections, 24 and 6 radiation lengths thick, the latter providing rejection against hadrons. The light from each section is collected by two BBQ-doped light guides on opposite sides of the cell.

In order to implement a trigger sensitive to electrons of high transverse momentum, the PM gains in all calorimeters were adjusted so that their signals were proportional to the transverse energy. Because of the cell dimensions, electromagnetic showers initiated by electrons may be shared among adjacent cells. Trigger thresholds were applied, therefore, to linear sums of signals from matrices of 2×2 cells, rather than to individual cells. In the central calorimeter, all possible 2×2 matrices were considered; in the two forward ones, we included only those made up of cells belonging to the same sector. A trigger signal was generated whenever the transverse energy deposition in at least two such matrices, separated in azimuth by more than 60°, exceeded a threshold corresponding to a transverse energy deposition of 3.5 GeV.

All calorimeters have been calibrated in a 10 GeV beam from the CERN PS, using incident electrons and muons. The stability of the calibration has since been monitored using a light flasher system, a Co^{60} source and a measurement of the average energy flow into each module for unbiased $\bar{p}p$ collisions [6]. The systematic uncertainty in the energy calibration of the electromagnetic calorimeters for the data discussed here amounts to an average value of ±1.5%. The cell-to-cell calibration uncertainty has a distribution with an rms of 3%.

The response of the calorimeters to electrons, and to single and multi-hadrons, has been measured at the CERN PS and SPS using beams from 1 to 70 GeV/c. In particular, both longitudinal and transverse shower developments have been studied, as well as the effect of particles impinging near the cell boundaries. The energy resolution for electrons is measured to be $\sigma_E/E = 0.14/\sqrt{E}$ (E in GeV).

3. Data analysis. The full data sample consists of approximately 7×10^5 triggers, which correspond to an integrated luminosity $L = 131$ nb^{-1}.

An initial selection is made by rejecting all events which are identified as due to sources other than $\bar{p}p$ collisions (<10% of the entire sample, mainly beam–gas background and cosmic rays). In the surviving events, a search is made for configurations consistent with the presence of electrons among the collision products. An electron is identified from the observation of:

(a) A track measured in the wire chambers.

(b) A large signal detected in the preshower counters (C5 in the central detector or the MTPCs in the two forward regions).

(c) An energy deposition in the calorimeters with small lateral sizes and limited penetration into the hadronic compartments.

And from the quality of the matching in space among these three properties.

Since the primary goal of this analysis is the detection of process (1), we first reduce the data sample by requiring the total electromagnetic transverse energy to exceed 30 GeV and the presence of a pair of energy clusters having an invariant mass in excess of 50 GeV/c^2 as calculated in the following way.

In the central calorimeter clusters are obtained by joining all electromagnetic cells which share a common side and contain at least 0.5 GeV. A contribution from the cells having at least one side in common with a cluster cell is also added.

The forward calorimeter clusters consist of at most two adjacent cells having the same azimuth (here the cell is far from the interaction point and much larger than the lateral extension of an electromagnetic shower, and the dead region between cells at different azimuths is too large to allow clustering across it).

In both cases the cluster energy E_{cl} is defined as $E_{cl} = E_{em} + E_{had}$ where E_{em} is the sum of the energies deposited in the electromagnetic compartments of the cluster cells and E_{had} is the corresponding sum for the hadronic compartments.

The invariant mass is calculated under the assumption that the event vertex is at the centre of the apparatus. We use the cluster centroids to define the momenta.

The remaining data sample contains 7427 events.

These events are then fully reconstructed and their invariant mass M is calculated again, this time taking into account the exact position of the event vertex. The difference between this new value and the previous one does not exceed 2 GeV/c^2.

At this stage the event sample is dominated by two-jet events [11]. However, while E_{cl} measures correctly the energy of jets produced in the central region, it is in general a gross underestimate of that of forward jets, for which the calorimeter thickness is only 88% of an absorption length. As a consequence, the sample contains many more events having both clusters in the central calorimeter than events with at least one cluster in the forward regions, because the jet momentum distribution falls off steeply with increasing jet transverse momentum [11].

In order to select events with similar characteristics in the central and forward regions and to enhance the electron signal, we further reduce the sample by requiring that both clusters have a small lateral size in the electromagnetic compartment of the calorimeter and a limited energy leakage in the hadronic compartment.

For clusters in the central calorimeter, cluster sizes R_θ, R_ϕ are calculated from the cluster centroid and the values of the angles θ and ϕ at the cell centres, weighted by their energy depositions. The conditions $R_\theta, R_\phi < 0.5$ cell sizes are required.

In the two forward calorimeters we require that the sum of the energies deposited in the cells adjacent to the cluster cells does not exceed 3 GeV.

The condition that the showers have only a small energy leakage in the hadronic compartments of the calorimeters is applied by requiring that the ratio $H = E_{had}/E_{cl}$ does not exceed a value H_0, equal to 0.02 for the forward calorimeters, and $0.023 + 0.034 \times \ln E_{cl}$, where E_{cl} is in GeV, for the central one.

The cuts applied at this stage are very loose and are satisfied by more than 95% of isolated electrons between 10 and 80 GeV, as verified experimentally using test beam data. They reduce the event sample to 24 events, whose invariant mass distribution is shown in fig. 2a. There are 12 events with both clusters in the central region, 8 events with one cluster in the central and the other in the forward regions, and 4 events with both clusters in the forward regions.

The sample with both clusters in the central region has been reduced by a factor ~430 by the cuts on cluster size and hadronic leakage.

In the following step we define a series of additional criteria for electron identification. We use measurements of the response of various parts of the de-

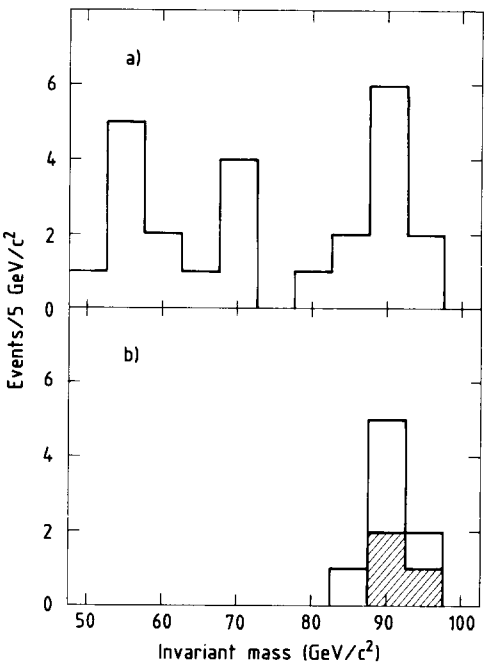

Fig. 2. Invariant mass distributions (a) of the 24 pairs which pass cut 1 of table 1, (b) of the eight of these 24 pairs for which all cuts of table 1 are satisfied by at least one electron. The three events in which both electrons pass all cuts of table 1 are cross-hatched.

Table 1
Electron identification criteria.

REQUIREMENTS	CENTRAL REGION		FORWARD REGIONS	
	Description	η(%)	Description	η(%)
1. Presence of a calorimeter cluster (preselection)	Electromagnetic cluster size $R_{\theta,\phi} < 0.5$ Hadronic leakage : $H < .023 + .034 \ln E_{cl}$	98	Cluster size ⩽ 2 cells Energy in adjacent cells $E_{adj} < 3$ GeV Hadronic leakage $H < 0.02$	98
2. Presence of a track	Reconstructed in the vertex detector in both transverse and longitudinal projections	85	Reconstructed a) in the vertex detector in transverse projection with $N \geq 1$ signal in the two inner chambers b) in the forward drift chambers. Azimuth difference between a) and b) $\Delta\phi$(a,b) less than 40 mrad	92
3. Track/cluster match	Track impact to cluster centroid distance $\Delta < 1$ cell size. Compare the energy distribution observed in the 3 × 3 cells centered on the impact cell to that expected for an electron incident along the track. Light sharing between phototubes of impact cell and hadronic leakage are taken into account. Require that the probability P that the energy distribution for an electron is farther from the mean than that observed is larger than 0.01	95	Shower position calculated from light sharing between impact cell phototubes must be consistent with the track impact point to within $\Delta x \leqslant 70$ mm	98
4. Presence of a preshower counter signal	Measured in C5 as a coincidence in space of charge clusters measured on the anode wires and the inner and outer cathode strips. Its charge q_5 must exceed 4 mip.	a) >90	Measured in MTPC in both coordinate planes. Its charge Q(MTPC) must exceed 6 mip	95
5. Track/preshower position match	Within d ⩽ 7 mm measured on the C5 surface	94	Within Δx, $\Delta y < 50$ mm in each direction	100
6. Momentum measurement			Momentum p measured in spectrometer and energy E measured in calorimeter must satisfy $\lvert p^{-1}-E^{-1}\rvert / \sigma (p^{-1}-E^{-1}) < 3$	99

a) This does not include a 5% inefficiency due to a $\Delta\phi = 18^{\circ}$ azimuthal region in which C5 was not operational because of electrical breakdown.

tector to isolated electrons [6,9,10] from which we evaluate approximate cut efficiencies η. The cuts are described in table 1 for both the central and forward regions. The efficiencies resulting from the simultaneous application of all selection criteria are at least as large as the products of the individual efficiencies η, namely 67% for the central region and 83% for the forward regions.

We have studied the effect of applying these criteria to our original event sample. We find that the rejection power of any one of these cuts enters as the square when applied to both clusters simultaneously. Furthermore the shape of the mass distribution shows no dependence, within statistics, on the combination of cuts used. These two observations provide a simple method to estimate the background contribution from two-jet events to any mass region in a sample of events surviving a given combination of cuts.

Fig. 2b shows the mass distribution for the events of fig. 2a with at least one cluster satisfying all of the electron identification criteria. There are eight events in this plot which cluster around a mass value of ~90 GeV/c^2. A list of relevant parameters for these events (named A–H) is given in tables 2 - 4. For clusters passing cut 3 of table 1 the cluster energy has been corrected to account for the calorimeter response as a function of the electron incidence angle and impact point. The corrected energy value, together with the measured track direction, has been used to calculate the invariant mass plotted in figs. 2a and 2b.

An upper limit on the background contribution to the eight events in fig. 2b can be inferred from fig. 2a under the assumption that background events have the same mass distribution in both samples. By comparing the event populations above and below 80 GeV/c^2 we find an upper limit (90% CL) of 0.32 background

Table 2
Event parameters.

Event	A	B	C	D	E	F	G	H
Pair Configuration C = central F = forward	CF	CC	CF	CF	CF	CC	CC	CC
Pair Mass (GeV/c^2)	90.7 ±2.1	95.2 ±3.4	89.7 ±2.8	89.1 ±3.2	94.0 ±2.9	89.3 ±4.9	83.2 a) ±2.6	88.3 a) ±2.6
Pair Transverse Momentum (GeV/c)	5.0	11.9	1.4	2.4	4.6	5.0	7.9	6.2

a) Ignoring additional energy measured in neighbour cells.
Its inclusion results in a mass increase of $\sim$ 3 GeV/c^2.

events to the signal in fig. 2b. However, this allows for up to 2.3 low mass events ($M < 80$ GeV/c^2) in fig. 2b – while in fact we observe none – and may result in a substantial overestimate of the background.

A better estimate implies a more realistic evaluation of the expected number of low mass background events in fig. 2b. This can be done starting from a much richer event sample by simply releasing cut 1 (hadronic leakage and cluster size) on one of the two clusters and evaluating the rejection power of cuts 2–6 (applied to reduce the sample of fig. 2a to that of fig. 2b) on the other cluster. We have checked that the absence of significant correlation between the fragmentations of the two jets in background events makes this procedure legitimate. Also we have taken advantage of the fact that all events in fig. 2b have at least one central cluster to restrict the operation of releasing cut 1 to central clusters exclusively. In this way we estimate a background contribution of 0.03 events to the signal of fig. 2b.

If we apply the electron identification criteria to both clusters, only three events (A–C, shown as cross-hatched areas in fig. 2b) survive, with an estimated background of 2×10^{-4} events above a mass of 80 GeV/c^2. For two of them (A and C) one of the electrons is in the forward regions, the other electrons are in the central region. Events A and B are interpreted as resulting from reaction (1). Event C consists of two electrons and a well separated high energy photon (or unresolved photons such as from the $\gamma\gamma$ decay of a π^0 or η meson). The invariant mass value in table 2 and in fig. 2b is calculated for the three particles. We have estimated [11] that $Z^0 \to e^+e^-\gamma$ decays with a photon at least as hard as the observed one, and with e^+e^- opening angles equal to, or smaller than the measured one occur approximately once every 200 $Z^0 \to e^+e^-$ decays.

Fig. 3a shows the longitudinal view of event A in the plane containing the central electron. Figs. 3b and 4a show the cell energy distribution in θ and ϕ for events A and C. The transverse view of event C, indicating the presence of the additional photon at an angle of $\sim 30^\circ$ to the electron, is shown in fig. 4b.

We next discuss the five other events (D–H), in which one of the two electron candidates fails at least one of the strict selection criteria described in table 1.

– The forward electron candidate of event D is associated with a track measured in the vertex detector as pointing to a coil of the magnet at a place where its thickness is $\sim$0.5 radiation lengths. Three tracks, measured in the forward drift chambers, point to the energy cluster. One of them passes cut 2 but fails cut 6. Several MTPC clusters satisfy cut 4, but cuts 3 and 5 are never simultaneously satisfied (table 3). This configuration is consistent with the hypothesis of an electron initiating an electromagnetic shower in the magnet coil. The mass value listed in table 2 has been calculated under this hypothesis. Event D belongs to the data sample collected in 1982 and has been previously published [12].

– The central electron candidate of event E passes all strict cuts but 4 and 5 (table 4). Its associated C5 cluster has a charge of only 2.4 mip and is 9 ± 2 mm away from the track impact. The occurrence of such a configuration in the present sample is compatible with the cut efficiencies listed in table 1 and event E is consistent with an electron pair hypothesis. We note however that the forward electron is accompanied by

[11] We thank R. Petronzio for assistance in making this calculation (to first order in α).

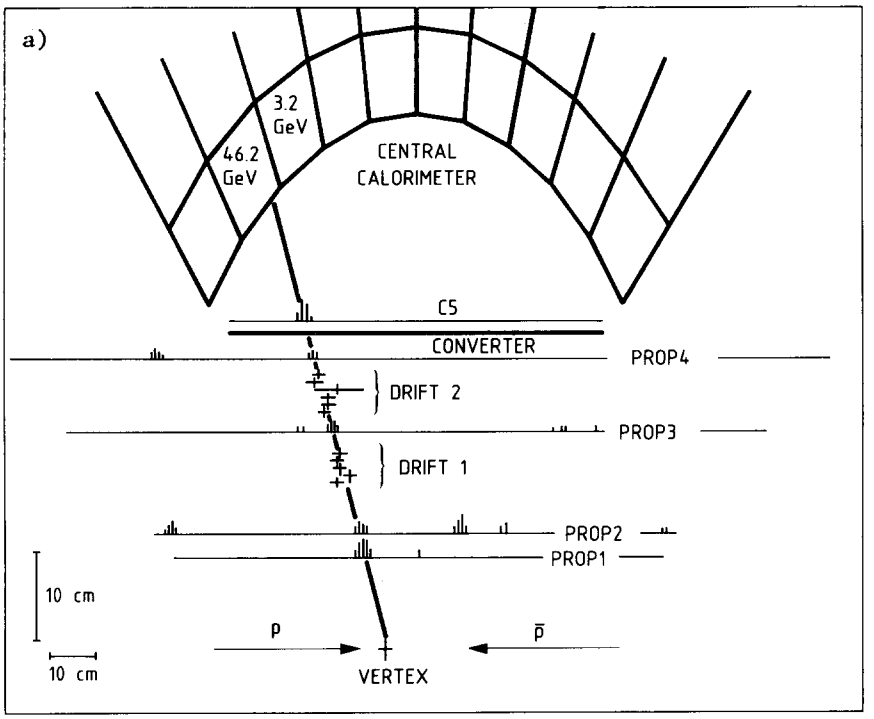

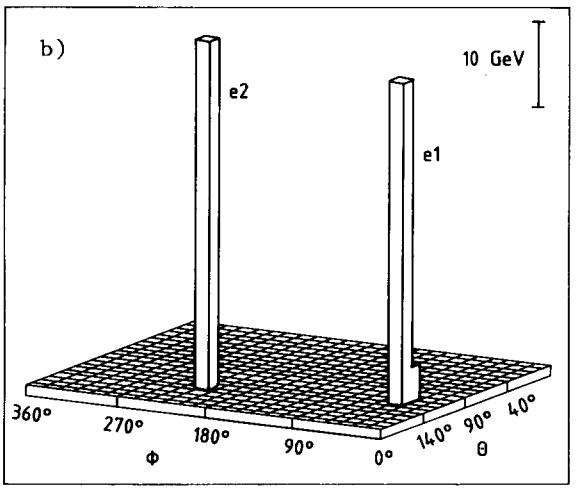

Fig. 3. (a) Longitudinal view of event A in the plane containing the central electron. In each of the four proportional chambers of the vertex detector (PROP 1–4) and in the preshower chamber C5 located behind the tungsten converter, signals are indicated whenever a coincidence in space was observed between the anode wire and the inner and outer cathode strips. The measurements from the two drift chambers (DRIFT 1 and 2) are indicated as crosses with sizes corresponding to the uncertainty on the charge division measurement. Energies measured in the electromagnetic cells facing the electron track are indicated, when non zero. (b) The cell transverse energy distribution for event A in the (θ, ϕ) plane.

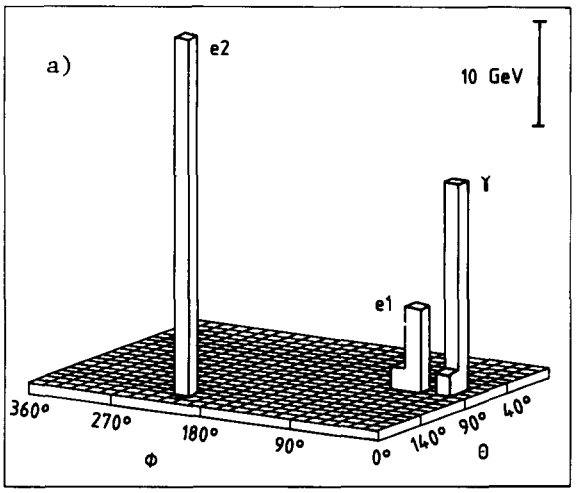

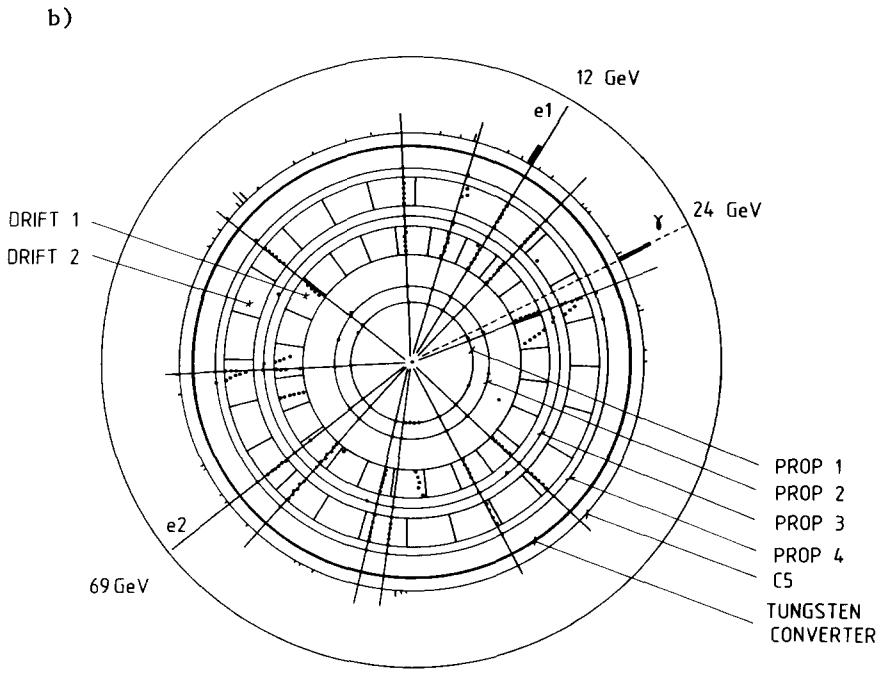

Fig. 4. (a) The cell transverse energy distribution for event C in the (θ, ϕ) plane. Electron e1 and the photon (γ) are observed in the central region, electron e2 in the forward region. (b) The transverse view of event C. Signals from the proportional and drift chambers are indicated as dots. Electron e1 and the photon (γ) are observed in the central region and associated with C5 signals (indicated by heavy lines proportional to pulse height). Electron e2 is observed in the forward region (not covered by C5).

Table 3
Electron parameters (forward regions).

Cut (see Table I)	Event	A	C	D	E
	θ (degrees)	142.2	150.3	155.8	148.3
	φ (degrees)	218.6	219.9	324.3	173.4
	E (GeV)	70.4 ± 1.6	68.5 ± 1.6	99.2 ± 6.0	58.1 ± 1.7
	I (mip)	0.9	0.9	1.9	0.9
1	Eadj (GeV)	0	0	3.0	0
	H (%)	0.4	0.7	0.4	0.3
2	Δφ(a,b) (mrad)	2	2	7	8
	N	2	2	2	2
3	Δx (mm)	11	29	81 [a]	60
4	Q (MTPC) (mip)	> 64	14	19	> 42
5	Δx (mm)	1.4	5.0	40.5	1.0
	Δy (mm)	1.8	4.7	8.8	2.1
6	$\frac{\lvert p^{-1}-E^{-1}\rvert}{\sigma(p^{-1}-E^{-1})}$	0.40	0.15	29.50 [a]	0.09

[a] This value fails the corresponding cut.

another particle having a measured momentum of 2.3 GeV/c and hitting the same calorimeter cell. The mass value listed in table 2 has been corrected accordingly. In minimum bias events the probability that a particle with a measured momentum >2.3 GeV/c hits a given calorimeter cell of the same θ is only 0.2%.

– One of the central electron candidates of event F passes all strict cuts but cut 3. The measured ratio of the signals from the two light guides of the impact cell is 0.71 ± 0.02 instead of 0.88 ± 0.02 as predicted from the track impact. Nothing suspicious has been found in the behaviour of the calorimeter cell from the monitoring of the stability of its calibration using light flasher and Co^{60} source measurements. We have also checked that the ratio between the light transmitted by the two light guides has the expected distribution in minimum bias events. Event F could be compatible with an electron pair hypothesis if a neutral particle (for example a hard bremsstrahlung photon) had entered the calorimeter cell very near its edge (~70 mrad away from the electron) causing many shower particles to cross the associated light guide. However the absence of a C5 cluster facing this region would imply that the photon did not convert in the 1.5 radiation lengths thick converter.

– The electron candidates of events G and H which do not pass the strict cuts are both observed in the central region. The latter fails cut 4 because it happens to fall in the small region ($\Delta\phi = 18°$) where C5 is non operational. We ignore this fact in the present discussion. Both fail cut 3 for the following reason: additional energy (~3 GeV) is observed in neighbour cells, inconsistent with lateral and longitudinal leakages of a shower initiated by an electron of the measured energy. In both cases this additional energy has an important component in the hadronic compartments: it is therefore difficult to ascribe it to radiative effects. We observe no track pointing to these cells, and no C5 cluster facing them. In the case of minimum bias events superimposed at random on large transverse momentum identified electrons we find that the probability of observing similar configurations is about 0.1%. We have also checked, using the light flasher system, that cross-talk between neighbour cells is negligible.

The presence of additional energy in these events has been ignored when calculating the invariant mass (table 2 and fig. 2). From the above discussion we retain the following points:

(a) Eight events (A–H) are observed with at least one electron passing the strict identification criteria. Their masses cluster in the 90 GeV/c^2 region where the expected background is only 0.03 events.

(b) Five of these events (A–E) are either identified as, or perfectly compatible with, e^+e^- or $e^+e^-\gamma$ configurations.

(c) The three other events (F–H) have both clus-

Table 4
Electron parameters (central region).

Cut (see Table I)	Event	A	B		C		D	E	F		G		H	
	θ(degrees)	117.4	61.2	45.9	81.8	79.0	126.4	44.3	132.4	98.1	126.8	104.8	115.0	67.4
	φ(degrees)	38.3	299.7	130.2	59.5	27.7	147.2	1.7	123.3	306.4	346.6	162.2	198.6	27.0
	E(GeV)	49.5 ±2.0	48.3 ±2.3	73.2 ±4.0	11.4 ±0.9	24.4 ±1.4	50.8 ±2.0	38.6 ±2.1	53.0 ±5.5	46.0 ±1.8	45.0 ±1.8	47.5 ±2.3	46.5 ±2.0	42.1 ±1.7
	I(mip)	1.2	1.2		0.8		1.7	1.4	1.7	1.3	1.3	1.4	0.9	1.8
1	Max(R_θ,R_ϕ) (cell sizes)	0.25	0.36	0.39	0.39	0.26	0.31	0.40	0.16	0.38	0.36	0.16	0.13	0.12
	H(%)	6.5	5.0	12.9	5.0	8.9	8.1	6.2	10.8	8.7	8.9	3.1	10.6	4.4
3	Δ(cell sizes)	0.22	0.46	0.21	0.43		0.35	0.33	0.26	0.24	0.50	0.36	0.27	0.44
	P(%)	35	28	11	6	67	15	69	0.001[a]	83	0[a]	28	0.002[a]	60
4	q_5(mip)	14.5	24.8	23.8	13.9	29	4.5	2.4[a]	5.3	20.4	16.5	105.6	–[a]	31.6
5	d(mm)	3.2	1.8	0.9	1.5	— (γ)	1.9	8.9[a]	5.6	1.2	0.2	2.6	–[a]	3.2

[a] This value fails the corresponding cut.

ters in the central region. In each of these events one cluster fails cut 3. Although we retain the interpretation that this cluster is in each case associated with an electron, its configuration is inconsistent with our present knowledge of the detailed response of the central calorimeter to high energy electrons. However, we shall repeat the measurements of relevance in a high energy electron beam before drawing any definite conclusion on the significance of these inconsistencies.

The presence in fig. 2b of a signal free of background contamination, and the difficulties encountered in interpreting events F–H in terms of electron pairs, have led us to consider the hypothesis that the sample of fig. 2b could be contaminated by a background peaking in the (W, Z^0) mass region, but not made of genuine electron pairs. W and Z^0 decay modes other than $e^\pm\nu$ and e^+e^- (for example into two hadron jets) could provide such a mechanism. However we find it difficult to retain such an hypothesis because the sample of fig. 2a contains only two extra events, compatible with the background expectation of 0.7 events, in the mass region above 80 GeV/c^2.

4. Conclusions. The most likely interpretation of the eight events in fig. 2b is that they all result from the decays $Z^0 \to e^+e^-$ or $Z^0 \to e^+e^-\gamma$.

However three of these events (F–H) are not completely consistent with this hypothesis. Event D contains an electron for which the energy is not accurately measured. We restrict therefore the following discussion to the sample of four events (A–C and E) which can be used with confidence in an evaluation of the Z^0 mass and width.

From these events we measure the mass of the Z^0 boson to be:

$$M_Z = 91.9 \pm 1.3 \pm 1.4\ \text{GeV}/c^2, \qquad (2)$$

where the first error accounts for measurement errors and the second for the uncertainty on the overall energy scale.

The rms of this distribution is 2.6 GeV/c^2, consistent with the expected Z^0 width [13] and with our experimental resolution of ~3%.

Under the hypothesis of Breit–Wigner distribution we can place an upper limit on its full width

$$\Gamma < 11\ \text{GeV}/c^2 \quad (90\%\ \text{CL}), \qquad (3)$$

corresponding to a maximum of ~50 different neutrino types in the universe [14].

The standard SU(2) × U(1) electroweak model makes definite predictions on the Z^0 mass. Taking into account radiative corrections to $O(\alpha)$ one finds [13]

$$M_Z = 77\ \rho^{-1/2}(\sin 2\theta_W)^{-1}\mathrm{GeV}/c^2, \quad (4)$$

where θ_W is the renormalised weak mixing angle defined by modified minimal subtraction, and ρ is a parameter which is unity in the minimal model.

Assuming $\rho = 1$ we find

$$\sin^2\theta_W = 0.227 \pm 0.009. \quad (5)$$

However, we can also use the preliminary value of the W mass found in this experiment [15]

$$M_W = 81.0 \pm 2.5 \pm 1.3\ \mathrm{GeV}/c^2.$$

Using the formula [13]

$$M_W = 38.5\,(\sin\theta_W)^{-1}\mathrm{GeV}/c^2, \quad (6)$$

we find $\sin^2\theta_W = 0.226 \pm 0.014$, and using also eq. (4) and our experimental value of M_Z we obtain

$$\rho = 1.004 \pm 0.052, \quad (7)$$

in agreement with the prediction of the minimal SU(2) × U(1) model, with the recent results of the UA1 experiment [4], and with the results of low energy neutrino experiments [16].

This experiment would have been impossible without the collective effort of the staffs of the relevant CERN accelerators. They are gratefully acknowledged.

We are grateful to the UA4 Collaboration for providing signals for the luminosity measurement.

We are deeply indebted to the technical staffs of the Institutes collaborating in UA2 for their invaluable contributions.

Financial supports from the Schweizerischer Nationalfonds zur Förderung der Wissenschaftlichen Forschung to the Bern group, from the Danish Natural Science Research Council to the Niels Bohr Institute Group, from the Institut National de Physique Nucléaire et de Physique des Particules to the Orsay group, from the Istituto Nazionale di Fisica Nucleare to the Pavia group, and from the Institut de Recherche Fondamentale (CEA) to the Saclay group are acknowledged.

References

[1] S.L. Glashow, Nucl. Phys. 22 (1961) 579;
S. Weinberg, Phys. Rev. Lett. 19 (1967) 1264;
A. Salam, Proc. 8th Nobel Symp. (Aspenäsgården, 1968) (Almqvist and Wiksell, Stockholm) p. 367.
[2] G. Arnison et al., Phys. Lett. 122B (1983) 103.
[3] M. Banner et al., Phys. Lett. 122B (1983) 476.
[4] G. Arnison et al., Phys. Lett. 126B (1983) 398.
[5] UA2 Collab., B. Mansoulié, presented at XVIIIth Rencontre de Moriond on Proton–antiproton collider physics (La Plagne, March 1983), to be published.
[6] A. Beer et al., The central calorimeter of the UA2 experiment at the CERN $\bar{p}p$ collider, to be published in Nucl. Instrum. Methods.
[7] M. Banner et al., Phys. Lett. 115B (1982) 59.
[8] M. Banner et al., Phys. Lett. 122B (1983) 322.
[9] C. Conta et al., The system of forward–backward drift chambers in the UA2 detector, to be published in Nucl. Instrum. Methods.
[10] K. Borer et al., Multitube proportional chambers for the location of electromagnetic showers in the CERN UA2 detector, to be published in Nucl. Instrum. Methods.
[11] M. Banner et al., Phys. Lett. 118B (1982) 203;
P. Bagnaia et al., Measurement of production and properties of jets at the CERN $\bar{p}p$ collider, CERN-EP/83–94 (July 1983), submitted to Z. Phys. C.
[12] UA2 Collab., P. Darriulat, presented at Third Topical Workshop on $\bar{p}p$ collider physics (Rome, January 1983), CERN 83–04 (May 1983), eds. C. Bacci and G. Salvini (CERN, Geneva, 1983) pp. 235, 236.
[13] For a review see: M.A.B. Bég and A. Sirlin, Phys. Rep. 88 (1982) 1 and references quoted therein (in particular Section 4, references 27–39);
see also W.J. Marciano and Z. Parsa, Proc. AIPDPF, Summer Study on Elementary particle physics and future facilities (Snowmass, CO, 1982) (AIP, New York, 1983) p. 155;
M. Consoli, S. Lo Presti and L. Maiani, Higher order effects and the vector boson physical parameters, University of Catania preprint, PP/738-14/1/1983.
[14] J. Ellis, M.K. Gaillard, G. Girardi and P. Sorba, Ann. Rev. Nucl. Part. Sci. 32 (1982) 443, and references therein.
[15] UA2 Collab., G. Sauvage, preliminary results presented at Intern. Europhysics Conf. on High energy physics (Brighton, UK, July 1983);
UA2 Collab., A.G. Clark, at 1983 Intern. Symp. on Lepton and photon interactions at high energies (Cornell, USA, August 1983).
[16] For a recent review see: M. Davier, Supp. J. Phys. (Paris) 12, C3 (1982) 471, and references therein.